EPJ A
Hadrons and Nuclei

EPJ.org
your physics journal

Eur. Phys. J. A (2019) **55**: 236 DOI 10.1140/epja/i2019-12784-4

# Excitation of the electric pygmy dipole resonance by inelastic electron scattering

V.Yu. Ponomarev, D.H. Jakubassa-Amundsen, A. Richter and J. Wambach

Società Italiana di Fisica

Springer

Eur. Phys. J. A (2019) **55**: 236
DOI 10.1140/epja/i2019-12784-4

THE EUROPEAN PHYSICAL JOURNAL A

Regular Article – Theoretical Physics

# Excitation of the electric pygmy dipole resonance by inelastic electron scattering*

V.Yu. Ponomarev[1,a], D.H. Jakubassa-Amundsen[2], A. Richter[1], and J. Wambach[1,3]

[1] Institut für Kernphysik, Technische Universität Darmstadt, D-64289 Darmstadt, Germany
[2] Mathematisches Institut, Universität München, Theresienstraße 39, D-80333 München, Germany
[3] European Centre for Theoretical Studies in Nuclear Physics and related Areas (ECT*) and Fondazione Bruno Kessler, Villa Tambosi, 38123 Villazzano (TN), Italy

Received: 14 April 2019 / Revised: 23 May 2019
Published online: 3 December 2019

Communicated by N. Alamanos

*Dedicated to Pier Francesco Bortignon*

**Abstract.** To complete earlier studies of the properties of the electric pygmy dipole resonance (PDR) obtained in various nuclear reactions, the excitation of the $1^-$ states in $^{140}$Ce by $(e,e')$ scattering for momentum transfers $q = 0.1$–$1.2$ fm$^{-1}$ is calculated within the plane-wave and distorted-wave Born approximations. The excited states of the nucleus are described within the Quasiparticle Random Phase Approximation (QRPA), but also within the Quasiparticle-Phonon Model (QPM) by accounting for the coupling to complex configurations. It is demonstrated that the excitation mechanism of the PDR states in $(e,e')$ reactions is predominantly of transversal nature for scattering angles $\theta_e \approx 90°$–$180°$. Being thus mediated by the convection and spin nuclear currents, the $(e,e')$ like the $(\gamma,\gamma')$ reaction, may provide additional information to the one obtained from Coulomb and hadronic excitations of the PDR in $(p,p')$, $(\alpha,\alpha')$, and heavy-ion scattering reactions. The calculations predict that the $(e,e')$ cross sections for the strongest individual PDR states are in general about three orders of magnitude smaller as compared to the one of the lowest $2^+_1$ state for the studied kinematics, but that they may become dominant at extreme backward angles.

## 1 Introduction

A group of low-lying $1^-$ states in neutron-rich heavy nuclei below the particle emission threshold is often referred to as the Pygmy Dipole Resonance (PDR). The excitation probability of the PDR by photons is about two orders of magnitude smaller as compared to the Giant Dipole Resonance (GDR). Nonetheless the high selectivity of the electromagnetic interaction to the excitation of dipole states already allowed to observe the PDR in experiments with tagged photons as a bump of unresolved states with a width of about 2–3 MeV [1,2]. Later, nuclear resonance fluorescence (NRF) experiments with high resolution in Darmstadt [3] and Gent [4] and follow-up studies during the last 20 years also at the ELBE accelerator of the Helmholtz-Zentrum Dresden-Rossendorf [5] and at the High Intensity $\gamma$-ray Source (HI$\gamma$S) operated by Triangle University Nuclear Laboratory (TUNL) [6], identified the PDR fine structure, *i.e.* hundreds of $1^-$ states were observed in spherical nuclei at the PDR excitation energy.

Recently, other probes were used to investigate the PDR properties: $1^-$ states which form the PDR, were studied in $(\alpha,\alpha'\gamma)$ [7], $(p,p')$ [8], $(^{17}\mathrm{O},^{17}\mathrm{O}'\gamma)$ [9], and $(p,p'\gamma)$ [10] reactions, in which the detection of the $\gamma$ decay photon in coincidence with the scattered particle was used to select the corresponding excitation of a $1^-$ state. For example, the spectrum of the $1^-$ states in $^{208}$Pb obtained in the $(p,p')$ reaction at very small scattering angles ($\theta_{\mathrm{lab}} < 1°$, where the excitation process is purely determined by the Coulomb interaction between projectile and target [8]) resembles closely the NRF spectrum [11]. At the same time, Coulomb and strong ($NN$) interactions between projectile and nucleus play an important role in the excitation of the PDR states in the other reactions mentioned above. As a result of the different sensitivity

* Contribution to the Topical Issue "Giant, Pygmy, Pairing Resonances and Related Topics" edited by Nicolas Alamanos, Ricardo A. Broglia, Enrico Vigezzi.

[a] e-mail: ponomare@theorie.ikp.physik.tu-darmstadt.de

of various reactions, some $1^-$ states are observed in NRF spectra but not in reactions with hadronic probes and vice versa. Also, the relative excitation strengths of different individual states deviate appreciably. Contrary to the GDR states where the $E1$-strength is concentrated merely in a single collective level called 1p-1h doorway state and a spreading over many states of 2p-2h, 3p-3h, ... character (see, *e.g.*, [12]), the PDR is characterized by probably a few doorway states. We will return to this point in some detail below.

For a detailed account of the present status of studies of the PDR properties we refer to a recent review article [13].

In the present work we consider the possibility of using electrons as a projectile to supply further information on the properties of the $1^-$ states belonging to the PDR. As it will become clear from results presented below, the prerequisite for an experimental verification of them are the availability of i) low energy electron beams and ii) high-resolution and large acceptance magnetic spectrometers. Both conditions are, *e.g.*, fulfilled at the S-DALINAC (Superconducting DArmstadt electron LINear ACcelerator) and its spectrometers LINTOTT and Q-CLAM [14]. Some selective excitations of isoscalar and isovector electric dipole transitions below the electric giant resonance region were, *e.g.*, investigated in $^{12}$C, $^{16}$O, $^{40}$Ca and $^{208}$Pb [15–18]. Furthermore, some benchmark high-resolution $(e, e'x)$ experiments with $x = p, n, \alpha$ and the decay of the Giant Dipole Resonance in the doubly magic nuclei $^{40}$Ca and $^{48}$Ca were also performed at the S-DALINAC [19–23] but in general, the information on the observation of detailed strength distributions of $1^-$ states in the $(e, e')$ reactions is very sparse.

Concerning the physical origin of low energy electric dipole strength and its particular distribution we note in passing that there exists at present still no clear picture about the relevant excitation mechanism. Recent self-consistent Random-Phase Approximation (RPA) calculations with various finite-range forces in $^{16}$O and $^{40}$Ca [24] and also $^{48}$Ca [25] have shown that, *e.g.*, nuclear surface vibrations might mix with skin modes and thus influence the pygmy dipole strength. It is stated clearly there that an electroexcitation experiment of the $(e, e')$ type could eventually help to "improve the different models aspiring to describe reliably the low-energy dipole strength of nuclei" [25]. This point has also been independently emphasized in [26]. To provide some estimates for the feasibility of $(e, e')$ experiments is the main purpose of this article.

The cross section for the excitation of natural parity states in $(e, e')$ reactions has a longitudinal and transversal component. It is expected that the longitudinal or Coulomb term gives rise to a distribution of electric dipole strength over energy quite similar to the one seen in NRF experiments, at least at small momentum transfer. However, the transversal part is mediated by nuclear currents, and thus provides an alternative mechanism to excite the same set of PDR states in addition to the Coulomb and $NN$ excitations.

It is thus important

- to investigate at which kinematics the transversal mechanism dominates over the longitudinal one in the excitation of the PDR states, and to compare it to the behaviour of the excitation of the collective GDR and
- to provide realistic estimates of the $(e, e')$ cross section for the excitation of the PDR levels.

Electrons with incident kinetic energies from 30 to 120 MeV will be considered. Such energies can be provided by the S-DALINAC in Darmstadt, where the detector system allows for measurements in a wide range of scattering angles, including backward scattered electrons close to 180° which can be detected with high angular resolution [14,27].

The calculations have been performed for $^{140}$Ce, a semi-magic nucleus in which the PDR has already been studied in $(\gamma, \gamma')$, $(p, p')$, and $(\alpha, \alpha')$ reactions [10].

## 2 Plane-wave Born approximation

The theory of inelastic scattering of electrons on nuclei is well developed and may be found in textbooks (see, *e.g.*, [28]). The plane-wave Born approximation (PWBA) is usually sufficient for simple estimates. In the PWBA, the differential $(e, e')$ cross section for excitation of a natural parity state of multipolarity $\lambda$ can be written as [29]

$$\left(\frac{\mathrm{d}\sigma}{\mathrm{d}\Omega}\right)_\lambda \propto \left\{ V_L(\theta_e) \left|F_\lambda^C(q)\right|^2 + V_T(\theta_e) \left|F_\lambda^E(q)\right|^2 \right\}, \quad (1)$$

where $V_L(\theta_e)$ and $V_T(\theta_e)$ are the longitudinal and transversal kinematic factors, respectively, and $\lambda$ denotes the multipolarity of the transition. Nuclear structure information on the excited state enters via the charge transition density $\rho_\lambda(r)$ into the Coulomb form factor

$$F_\lambda^C(q) \propto \int_0^\infty \rho_\lambda(r) j_\lambda(qr) r^2 \mathrm{d}r \quad (2)$$

and via the transition current densities $J_{\lambda,\lambda\pm1}(r)$ into the electric form factor

$$\begin{aligned} F_\lambda^E(q) &= F_{\lambda,\lambda-1}^E(q) + F_{\lambda,\lambda+1}^E(q) \\ &\propto \sqrt{\lambda+1} \int_0^\infty J_{\lambda,\lambda-1}(r)\, j_{\lambda-1}(qr) r^2 \mathrm{d}r \\ &\quad + \sqrt{\lambda} \int_0^\infty J_{\lambda,\lambda+1}(r)\, j_{\lambda+1}(qr) r^2 \mathrm{d}r, \end{aligned} \quad (3)$$

where $q$ denotes the three-momentum transfer and $j_\lambda(qr)$ is the spherical Bessel function. Any interference between Coulomb and electric form factors is neglected in the PWBA.

At small $q$-values, Siegert's theorem [30] may be applied, resulting in

$$F_\lambda^E(q) \approx \frac{E_x}{q} \sqrt{\frac{\lambda+1}{\lambda}}\, F_\lambda^C(q), \quad (4)$$

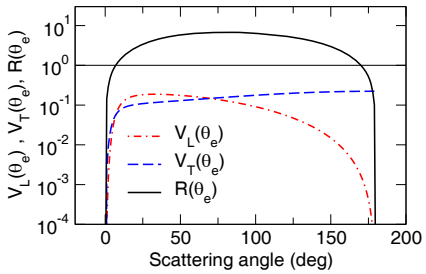


**Fig. 1.** Kinematic factors $V_L(\theta_e)$ and $V_T(\theta_e)$ in eq. (1) and the quantity $\mathrm{R}(\theta_e)$ in eq. (5) as function of the scattering angle $\theta_e$ for electrons with incident energy $E_e = 70\,\mathrm{MeV}$. See text for details.

where we have used relativistic units ($\hbar = c = 1$). When combining eqs. (1) and (4), the quantity

$$\mathrm{R}(\theta_e) = \frac{V_L^{1/2}(\theta_e)}{\frac{E_x}{q}\sqrt{\frac{\lambda+1}{\lambda}}\,V_T^{1/2}(\theta_e)} \qquad (5)$$

indicates whether the longitudinal or the transversal contribution dominates in the nuclear excitation process. This quantity is shown in fig. 1 by a solid line together with the kinematic factors $V_L(\theta_e)$ and $V_T(\theta_e)$. The calculation was performed for a hypothetical $1^-$ state with an excitation energy of $E_x = 8\,\mathrm{MeV}$ excited by $E_e = 70\,\mathrm{MeV}$ electrons. Notice that the excitation via the Coulomb form factor ($\mathrm{R}(\theta_e) > 1$) dominates in a wide range of scattering angles $\theta_e$, except for very forward ($\theta_e = 0°$–$8°$) and backward ($170°$–$180°$) angles.

When the momentum transfer $q$ is small, it is also possible to perform a Taylor expansion of the Bessel function $j_\lambda(qr)$ in eq. (2). Keeping only the first term, the square of the Coulomb form factor is closely related to the reduced transition probability $B(E\lambda)$ of the excited state, $|F_\lambda^C(q)|^2 \propto q^{2\lambda}\,B(E\lambda)$.

These simple estimates lead to the expectation that the distribution of $E1$ strength of states in the region of the PDR in $(e, e')$ experiments at small $q$-values is rather similar to the one in $(\gamma, \gamma')$ measurements. Indeed, at fixed kinematics, the $(\gamma, \gamma')$ excitation cross section is strictly proportional to $B(E\lambda)$ (see, *e.g.*, [31,32]). Some deviations are possible only at very large scattering angles of electrons.

The nuclear structure information on the states which form the PDR is contained in transition charge and current densities, which enter into eqs. (2) and (3). They were calculated for $^{140}$Ce within the quasiparticle-phonon model [33,34]. The model employs a nuclear Hamiltonian which includes the mean field for protons and neutrons (a phenomenological Woods-Saxon potential is usually used), monopole pairing, and residual interactions in a separable multipole form. Excitations of even-even nuclei are treated as quasi-bosons (phonons), the excitation energies and internal fermion structure of which are obtained by solving equations of motion of the quasiparticle random phase approximation (QRPA). This yields the eigenenergies and wavefunctions the one-phonon states.

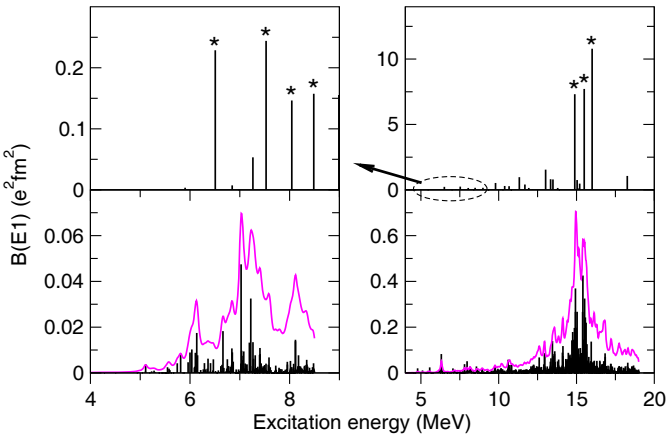


**Fig. 2.** The QPM prediction for the $B(E1)\uparrow$ strength distribution in $^{140}$Ce in the one-phonon approximation (top row) and accounting for the coupling to complex configurations: two-phonon (bottom right) and two- and three-phonon ones (bottom left). See text for details. The smooth curves in the bottom part (in relative units to guide the eye) are the result of an averaging over all states with a smearing parameter $\Gamma = 0.1\,\mathrm{MeV}$ (see eq. (9)). Selected one-phonon states for the discussion in the main text are marked by an asterisk.

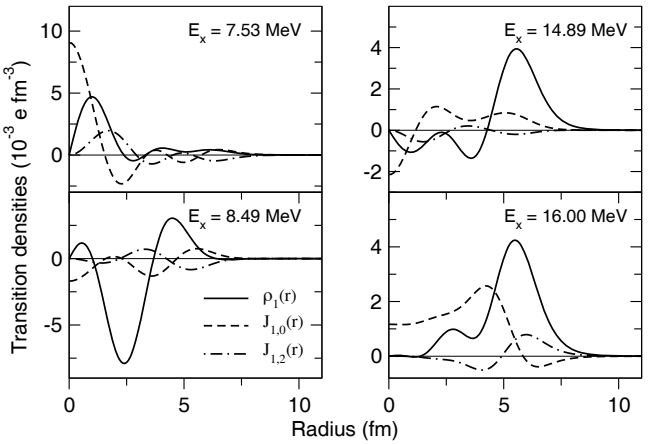


**Fig. 3.** Transition charge $\rho_1(r)$ (solid line) and current $J_{1,0}(r)$ (dashed line) and $J_{1,2}(r)$ (dash-dotted line) densities as a function of the radial coordinate $r$ for the excitation of some one-phonon $1^-$ states in $^{140}$Ce.

The distribution of the $B(E1)$ strength over the one-phonon $1^-$ states in $^{140}$Ce in the PDR energy region is shown in fig. 2(top-left). The states with the largest $B(E1)$ values are marked with an asterisk. They will be discussed in more detail below. Notice that their $B(E1)$ values are almost two orders of magnitude smaller as compared to the one-phonon states which form the GDR in fig. 2(top-right).

Transition charge density, $\rho_1(r)$, and current densities, $J_{1,0}(r)$ and $J_{1,2}(r)$, of some selected one-phonon $1^-$ states are presented in fig. 3 with their excitation energies indicated in the right-top corner of each panel. The ones belonging to the PDR (GDR) are shown in the left (right) column. The following effective charges for protons ($Z$)

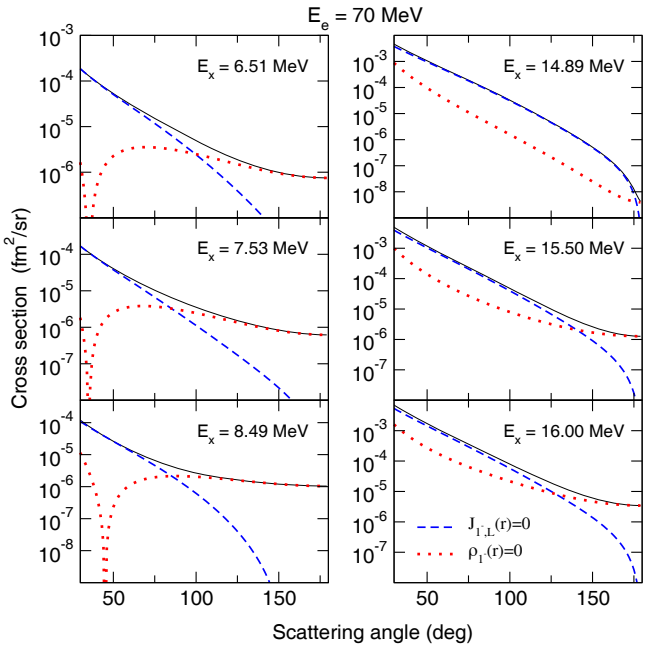


**Fig. 4.** Differential PWBA cross sections ($\mathrm{d}\sigma/\mathrm{d}\Omega$) for the excitation of one-phonon $1^-$ states from the PDR (left column) and the GDR (right column) energy region in $^{140}$Ce as a function of scattering angle $\theta_e$. The incident energy is 70 MeV. The longitudinal and transversal components are displayed as dashed and dotted lines, respectively. The total cross sections are shown by solid lines.

and neutrons ($N$) have been used: $e_{Z(N)} = N(-Z)/A$ for the $B(E1)$ values and charge densities, and the effective $g$-factors: $g_l^{Z(N)} = e_{Z(N)}$ for the convection current, and $g_s^{\mathrm{eff}} = 0.8\, g_s^{\mathrm{free}}$ for the magnetization current.

The charge transition densities of the $1^-$ states, which form the GDR, have a strong surface peaking, typical for collective vibrations. Protons and neutrons oscillate out of phase and due to different signs of the effective charges, they add constructively. The interference of 1p1h components in the wave function of one-phonon $1^-$ states from the PDR energy region has a destructive nature [35]. Their charge transition densities are peaking in the interior of the nucleus where their main 1p1h component is dominating. Accordingly, the position of minima and maxima varies from state to state.

The PWBA differential $(e, e')$ cross sections for the excitation of three selected one-phonon $1^-$ states, which belong to the PDR (GDR) are presented in the left (right) part of fig. 4 as a function of the angle of the scattered electrons. They are calculated for an incident energy of 70 MeV. The contribution of the longitudinal and transversal components is shown separately by dashed and dotted lines, respectively. Our conclusion about the longitudinal and the transversal contributions based on eq. (5) and fig. 1 remains valid for the GDR states. But for the PDR states the transversal component determines the excitation in a wide range of angles from 90° to 180°.

For all three PDR states the differential cross section has a very similar shape with deep minima between 40° and 50° and an almost flat behaviour for scattering angles $\theta_e > 70°$. The interplay between two terms of the electric form factor $F^E_{1,0}(q)$ and $F^E_{1,2}(q)$ in (3) is the source of those minima. The tails of the PDR current densities $J_{1,0}(r)$ at $r > 7$ fm lead to the sign change of the term $F^E_{1,0}(q)$ at low $q$ values creating the minima when $F^E_{1,0}(q) = -F^E_{1,2}(q)$. For the GDR states the term $F^E_{1,0}(q)$ always dominates over $F^E_{1,2}(q)$.

## 3 Distorted-wave Born approximation

Within the distorted-wave Born approximation (DWBA), one solves the Dirac equation for the incoming and outgoing electrons in the Coulomb field of the nucleus in terms of partial waves. Schematically, the differential cross section has the form

$$\left(\frac{\mathrm{d}\sigma}{\mathrm{d}\Omega}\right)_\lambda \propto \sum_{m_s,\mu} |A(\lambda\mu m_s)|^2\,, \qquad (6)$$

where $m_s$ and $\mu$ are the projections of the spin $\boldsymbol{s}$ of the incoming electron and of the angular momentum transfer $\boldsymbol{\lambda}$, respectively. The expression for the transition amplitudes $A(\lambda\mu m)$ may, *e.g.*, be found in [28,36]. An essential detail is that $A = A_C + A_E$, where both Coulomb ($A_C$) and electric ($A_E$) amplitudes are calculated by folding the nuclear charge and current transition densities, respectively, with the partial waves of the incoming and outgoing electron and with the propagator of the virtual photon. This implies that the DWBA accounts for the interference between two mechanisms for the excitation of natural parity states, (longitudinal) Coulomb and (transversal) electric.

One of the DWBA problems is a poor convergence of the radial integrals, particularly for dipole excitations at backmost scattering angles. We employ here the complex-plane rotation method developed in [37,38], to overcome this problem. This allows us to cover all scattering angles from 0° to 180°. The computation time is sped up by a multiple convergence acceleration in the sum over the final-state partial waves [39]. However, such an acceleration is not possible for angles $\theta_e \lesssim 10°$.

DWBA calculations have been performed for all one-phonon $1^-$ states of $^{140}$Ce with an excitation energy below 20 MeV (42 states in total). We have considered incident energies from 30 to 120 MeV and scattering angles from 40° to 180°. Special attention is paid to incident energies of 40, 70, and 110 MeV. They correspond roughly to the energies which may be achieved with the present set-up at the S-DALINAC after the beam passes the linac once, twice, and four times. The main results of the calculations are presented in figs. 5–8.

With figs. 5 and 6 we continue the discussion on the role of the longitudinal and transversal mechanisms of excitation which was started in connection with figs. 1 and 4. One state at 6.51 MeV belonging to the PDR (left column) and one at 15.50 MeV belonging to the GDR (right column) are considered in each of the figures. The dependence of the differential cross sections on scattering angle is presented in fig. 5 for the incident energies of 40, 70, and

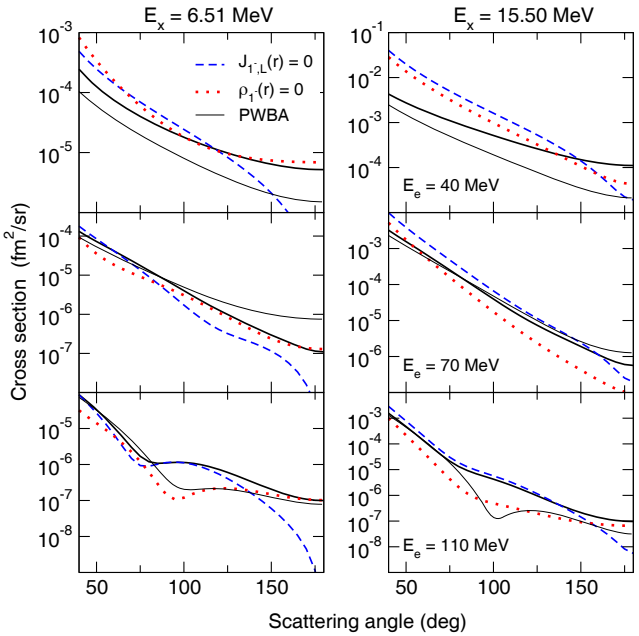


**Fig. 5.** Differential cross sections ($d\sigma/d\Omega$) for the excitation of the one-phonon $1^-$ states of energy 6.51 MeV (left column) and 15.50 MeV (right column) in $^{140}$Ce as a function of scattering angle $\theta_e$. The incident energy is 40 MeV (top row), 70 MeV (middle row), and 110 MeV (bottom row). The DWBA and PWBA results are represented by solid thick and thin lines, respectively. The results of the DWBA calculation in which only a "longitudinal" or "transversal" excitation is accounted for are displayed as dashed and dotted lines, respectively.

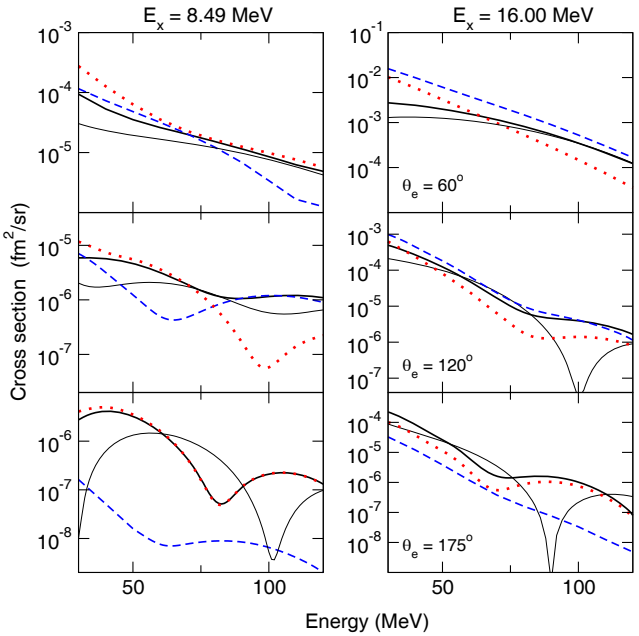


**Fig. 6.** Differential cross sections ($d\sigma/d\Omega$) for the excitation of the one-phonon $1^-$ states of energy 8.49 MeV (left column) and 16.00 MeV (right column) in $^{140}$Ce at a scattering angle 60° (top row), 120° (middle row), and 175° (bottom row) as a function of kinetic energy $E_e$ of the electrons. The definition of the lines is the same as in fig. 5.

110 MeV. The dependence on incident energy is shown in fig. 6 for the scattering angles 60°, 120°, and 175°. The DWBA cross sections are plotted by solid thick lines. By artificially setting $J_{1,L}(r) = 0$ or $\rho_1(r) = 0$ one obtains the excitation of the states by pure Coulomb (dashed line) or electric (dotted line) mechanisms, respectively.

The analysis of the results in figs. 5 and 6 yields conclusions similar to the ones drawn from the PWBA predictions in the previous section: the electric term in the excitation of the GDR plays the most important role only for very backward scattering, while for the PDR it may determine the cross section already at 90°. However, for some kinematics the interference between the Coulomb and electric parts may be extremely important (see, *e.g.*, right-top panel of fig. 5). In our examples this interference has often a destructive nature.

The DWBA results in figs. 5 and 6 are also compared to the PWBA predictions (thin solid lines). Basically, the DWBA leads to a smoothing of the sharp structures in PWBA due to the folding procedure. Although in some cases (*e.g.*, right-center panel of fig. 5) the agreement between the two approximations is rather good, in other cases they may disagree by an order of magnitude or more with each other.

Notice that summation over the partial waves in the DWBA completely washes out the deep minima in the transversal form factor of the PDR states at low $q$ discussed in the previous section.

Cross sections for the states marked with an asterisk in fig. 2 are plotted as a function of scattering angle (fig. 7) and as a function of bombarding energy (fig. 8). The selected states have the largest $B(E1)$ values in the PDR (left column) and GDR (right column) energy regions. The cross sections for other one-phonon $1^-$ states look rather similar except at the largest $q$-values in the studied kinematical range.

Low incident energies and small or modestly large scattering angles provide the biggest cross sections for the excitation of the PDR in inelastic electron scattering experiments. How large they are, can be seen from a comparison with the excitation cross sections for the $2_1^+$ and $3_1^-$ states (with excitation energies 1.596 MeV and 2.464 MeV, respectively) presented in the left panels of figs. 7 and 8 by solid and dotted lines. One notices that the one-phonon $1^-$ PDR states are about two orders of magnitude weaker excited in $(e, e')$ reactions than the $2_1^+$ state in a wide range of kinematics under consideration. An exception is the backmost scattering. The main reason is that for the excitation of the $2_1^+$ and $3_1^-$ states the transversal part plays a marginal role even at $\theta_e \to 180°$. It is sizeable, however, for the PDR states. But when changing the scattering angle from 40° to 180°, the PDR excitation cross sections drop by one to three orders of magnitude, depending on the incident electron energy.

## 4 Fine structure of the PDR

In order to discuss the absolute values of the $(e, e')$ excitation cross sections for the $1^-$ states in the PDR energy

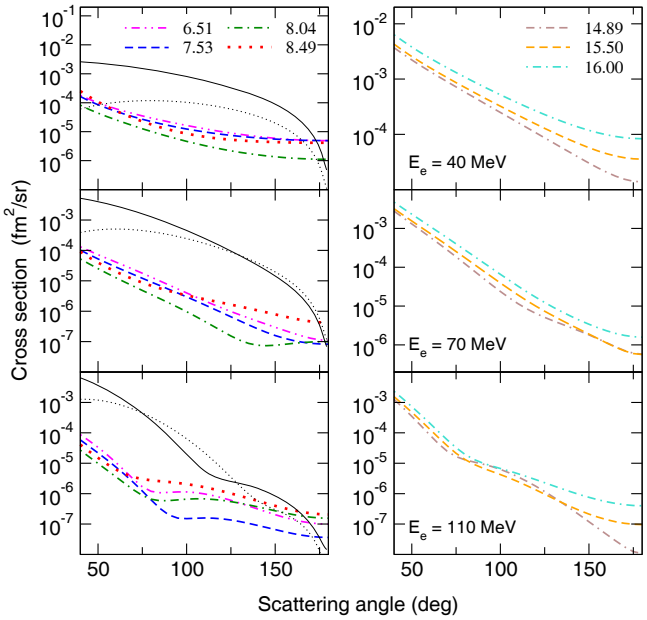


**Fig. 7.** Differential cross sections $(\mathrm{d}\sigma/\mathrm{d}\Omega)$ for the excitation of the selected one-phonon $1^-$ states from the PDR (left column) and GDR (right column) region in $^{140}$Ce as a function of scattering angle $\theta_e$. The incident energy is 40 MeV (top row), 70 MeV (middle row), and 110 MeV (bottom row). Excitation energies of the states are given in the inserts of the top row. Cross sections for the excitation of the $2^+_1$ (solid line) and $3^-_1$ (thin dotted line) states are plotted for comparison.

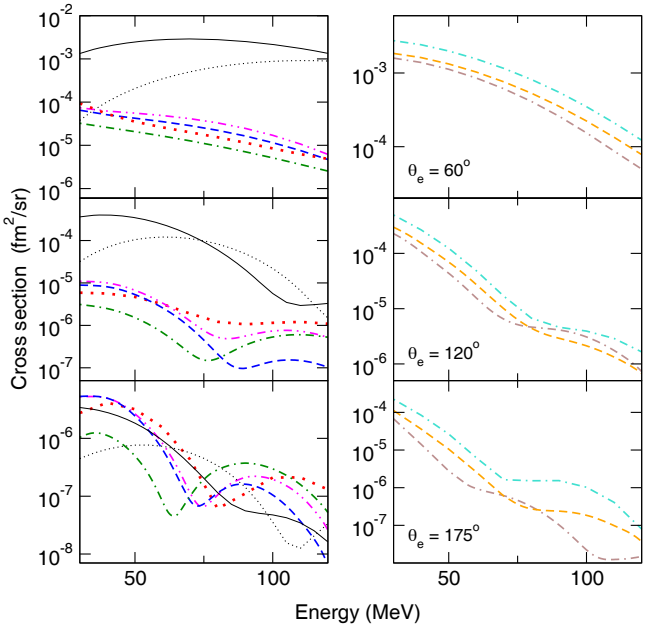


**Fig. 8.** Differential cross sections $(\mathrm{d}\sigma/\mathrm{d}\Omega)$ for the excitation of the selected one-phonon $1^-$ states in $^{140}$Ce at scattering angles 60° (top row), 120° (middle row), and 175° (bottom row) as a function of incident energy $E_e$ of the electrons. The definition of the lines is the same as in fig. 7.

region, which one expects to measure in an experiment, it is necessary to account for the fact that the one-phonon $1^-$ states, discussed in the previous sections, are embedded in more complex two-, three-, etc. phonon states. The excitation of the latter from the ground state is very weak as compared to the excitation of the one-phonon states, but their density increases rapidly with excitation energy. The interaction between the one-phonon and more complex states leads to a fragmentation of the strength carried by the one-phonon excitations into components from many states with more complex wave functions. In other words, we are dealing with the decay of the doorway one-phonon states owing to the interaction with more complex background states in the spirit of ref. [12].

In the QPM this decay is implemented by describing excited states with a wave function which contains one-phonon (first term), two-phonon (second term), and higher components

$$|\Psi^\nu_{\lambda\mu}\rangle = \Bigg\{ \sum_i R_i(\lambda\nu) Q^+_{\lambda\mu i} + \sum_{\lambda_1 i_1 \le \lambda_2 i_2} P^{\lambda_2 i_2}_{\lambda_1 i_1}(\lambda\nu) \times \Big[ Q^+_{\lambda_1\mu_1 i_1} Q^+_{\lambda_2\mu_2 i_2} \Big]_{\lambda\mu} + \cdots \Bigg\} |\Psi_{g.s.}\rangle, \quad (7)$$

where $Q^+_{\lambda\mu i}$ is the creation operator of a phonon with multipolarity $\lambda$ and its projection $\mu$, and where $i = 1, 2, 3 \ldots$ is the ordered number of the one-phonon states for a given $\lambda$. The phonon operators act on $|\Psi_{g.s.}\rangle$ which is the wave function of the ground state of even-even nuclei, identified with the phonon vacuum. Multiphonon configurations are built up of phonons of different multipolarities $(\lambda_1, \mu_1)$, $(\lambda_2, \mu_2)$, coupled to the same $(\lambda, \mu)$ as the one-phonon term

$$\Big[ Q^+_{\lambda_1\mu_1 i_1} Q^+_{\lambda_2\mu_2 i_2} \Big]_{\lambda\mu} = \sum_{\mu_1\mu 2} \langle \lambda_1\mu_1\lambda_2\mu_2 | \lambda\mu \rangle Q^+_{\lambda_1\mu_1 i_1} Q^+_{\lambda_2\mu_2 i_2}.$$

The eigenenergies of the states described by the wave functions (7), as well as the coefficients $R_i(\lambda\nu)$ and $P^{\lambda_2 i_2}_{\lambda_1 i_1}(\lambda\nu)$, are obtained by the diagonalization of the model Hamiltonian on the set of these wave functions. Since the model Hamiltonian is already prediagonalized on the QRPA level, one-phonon configurations do not interact with each other, but they mix in the wave function (7) due to their interaction with the same set of complex configurations.

The transition densities of the states (7) have the form of (7) where phonon operators are replaced by transition densities of one-, two-, etc. configurations. Neglecting the transition densities of the complex configurations, the cross section for excitation of the $\nu$-th $(\nu = 1, 2, 3, \ldots)$ state (7) in $(e, e')$ reactions can be written as

$$\left( \frac{\mathrm{d}\sigma}{\mathrm{d}\Omega} \right)_{\lambda\nu} \propto \sum_{m_s,\mu} \left| \sum_i R_i(\lambda\nu) A_i(\lambda\mu m_s) \right|^2, \quad (8)$$

where $A_i$ are the transition amplitudes for the $i$-th one-phonon state.

The first QPM calculation with the wave function (7) for the PDR states was performed for $^{140}$Ce in late 90-ies (see fig. 2 in ref. [3]) and compared to the results of one

of the first NRF experiment in which the fine structure of the PDR was observed. The model Hamiltonian was diagonalized in the basis of interactive one-, and a limited number of two-, and three-phonon configurations. The basis of complex configurations was extended later in [32]: two- and three-phonon configurations were built up from the phonons with multipolarities from $1^{\pm}$ to $9^{\pm}$ and were cut above 8.5 MeV. All 42 one-phonon $1^-$ configurations (discussed in the previous sections) were included in order to account for the GDR contribution at low excitation energies. The diagonalization yields 1157 $1^-$ states $\nu$ below 8.5 MeV. We will use this set of states in the discussion of the PDR below.

The fragmentation process of the $B(E1)$ strength of the doorway one-phonon $1^-$ states in the PDR energy region is demonstrated in the left part of fig. 2. To guide the eye, we also present in fig. 2(bottom) the strength function

$$S(B(E1), E_x) \propto \sum_{\nu} \frac{B_\nu(E1)}{(E_x - E_\nu)^2 + (\Gamma/2)^2} \qquad (9)$$

of the distribution where $E_\nu$ are the eigenenergies of the states (7) and $B_\nu(E1)$ are their reduced transition probabilities. The strength functions here are calculated with an artificial width $\Gamma = 0.1$ MeV and presented in arbitrary units.

The strongest states described by eq. (7) in fig. 2 (bottom) have $B(E1)$ values which are almost one order of magnitude smaller than the doorway ones in fig. 2(top). For the predictive power of the present set of the QPM wave functions we refer to fig. 2 in [10]. It combines information on excitation of the individual PDR levels in $^{140}$Ce as observed in $(\gamma, \gamma')$, $(p, p')$ and $(\alpha, \alpha')$ reactions in comparison with the calculation of the corresponding reaction cross sections performed with this set. Although it is not possible to establish a one-to-one correspondence between experiment and theory, a comparison of the calculations for single excitations in three different reactions with the experimental results on an absolute scale shows good agreement [10]. Also, calculations and experimental NRF data are found in good agreement concerning the degree of fragmentation and on the integrated strength, if the sensitivity limit of the experiments is taken into account [32]. All together, it leads us to expect that employing the same set of wave functions in the calculation of the $(e, e')$ cross sections will provide realistic values for the excitation of the strongest levels in the experiment.

The results of the DWBA calculations with the QPM wave functions eq. (7) are displayed in fig. 9 for an incident energy of 70 MeV and scattering angles 60°, 120°, and 180°. The strength functions in fig. 9 are defined similar to eq. (9) with the replacement of the $B_\nu(E1)$ quantities by the corresponding $(e, e')$ cross sections $(\mathrm{d}\sigma/\mathrm{d}\Omega)_\nu$, and are presented in arbitrary units which are different for different panels. As in the case of the $B(E1)$ quantities, the largest cross sections of an individual $\nu$-th state in fig. 9(left) are about one order of magnitude smaller than the cross sections of the doorway one-phonon states for the same kinematics.

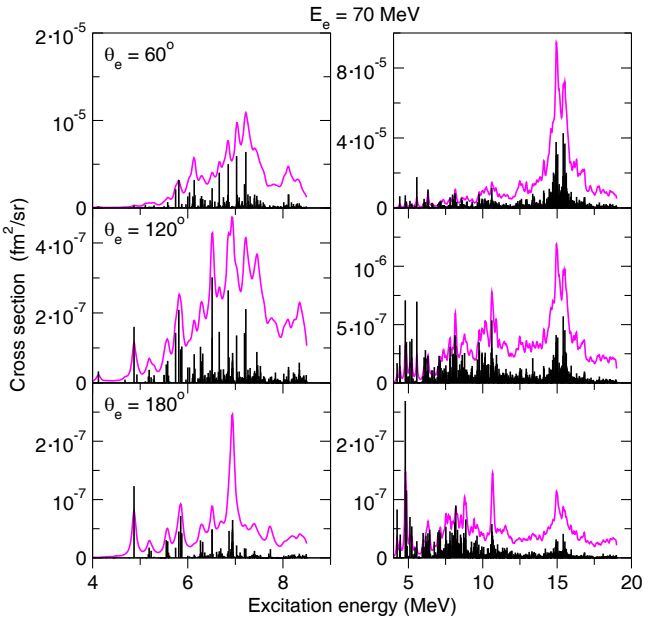


**Fig. 9.** Differential cross sections $(\mathrm{d}\sigma/\mathrm{d}\Omega)$ for the excitation of the $1^-$ states in $^{140}$Ce by electrons with incident energy of 70 MeV at scattering angles 60°, 120°, and 180° (from top to bottom). The calculations are performed with the QPM wave functions (7) which account for the coupling to complex configurations. Left column - the PDR, right column - the PDR and GDR. The strength functions are given by the smooth curves.

To discuss the relative $(e, e')$ cross sections in the excitation of the PDR and GDR, an additional diagonalization of the QPM Hamiltonian has been performed by extending the basis of two-phonon configurations up to 19 MeV. No three-phonon configurations have been accounted for in this calculation. The fine structure of the GDR strength is shown in fig. 2(right bottom) and fig. 9 for the $B(E1)$ values and $(e, e')$ cross sections, respectively.

Figure 9(left) demonstrates that, depending on the kinematics, the shape of the PDR excitation in inelastic electron scattering may vary dramatically and deviate from the distribution of the $B(E1)$ values which present the $q = 0$ limit. For some kinematics the summed cross sections of all PDR states from the $(e, e')$ reaction are even larger as compared to the summed ones for the GDR states. But the absolute values of the cross sections are small under such kinematical conditions.

## 5 Conclusion

The excitation of the $1^-$ states in $^{140}$Ce by inelastically scattered electrons with incident energies from 30 to 120 MeV is investigated. The scattering angle is varied from 40° to 180°. This kinematical range covers a momentum transfer $q$ from 0.1 to 1.2 fm$^{-1}$. We consider $1^-$ states which belong to the PDR and GDR. Their structure is described within the one-phonon QRPA, and by accounting for the coupling to complex configurations within the quasiparticle-phonon model.

It is demonstrated that Coulomb scattering is the dominant excitation mechanism for the GDR states in an $(e, e')$ reaction in a wide range of scattering angles, except for the very backward scattering. On the contrary, the PDR states are predominantly excited by transverse electric scattering mediated by the nuclear current for scattering angles in a large angular region from 90° to 180°. Also, the interference between the longitudinal and transversal components plays an important role for them. The latter effect is a distinctive feature of the DWBA calculations, while it is neglected in the PWBA.

The calculations show that the fine structure of the PDR in $(e, e')$ reactions may change substantially, depending on the kinematics, especially at large scattering angles. We predict that the $(e, e')$ excitation cross sections of the strongest individual $1^-$ states are about three orders of magnitude lower than the respective cross section for the $2_1^+$ state, except for very large scattering angles where the significant transversal contributions to the cross section for the PDR dominates. However, the absolute values of the cross section are rather small.

In this context we finally note that in earlier search for $M1$ and $M2$ giant resonances in $^{140}$Ce at the DALINAC the measured high-resolution spectra —$\Delta E$ varied between 28 and 48 keV (FWHM)— at backward angles showed no sign for excited $1^-$ states between excitation energies from 7.5 to 10 MeV [40], however, well resolved $1^-$ states in the region of interest have already been detected in $^{208}$Pb with an energy resolution of $\Delta E = 38$ keV FWHM [18]. With the improved electron beams from the S-DALINAC and its high-resolution spectrometers there is now, however, founded hope to detect them.

We thank Peter von Neumann-Cosel for discussions concerning the topic of the present studies. This work was supported by the Deutsche Forschungsgemeinschaft under Contract No. SFB 1245. We have dedicated this article to our late colleague and friend Pier Francesco Bortignon with whom we have discussed the physics of nuclear excitations for many years.

**Data Availability Statement** This manuscript has no associated data or the data will not be deposited. [Authors' comment: All data generated during this study are contained in this published article.]

**Publisher's Note** The EPJ Publishers remain neutral with regard to jurisdictional claims in published maps and institutional affiliations.

## References

1. R.M. Laszewski, P. Axel, Phys. Rev. C **19**, 342 (1979).
2. R.M. Laszewski, Phys. Rev. C **34**, 1114 (1986).
3. R.D. Herzberg, P. von Brentano, J. Eberth, J. Enders, R. Fischer, N. Huxel, T. Klemme, P. von Neumann-Cosel, N. Nicolay, N. Pietralla, V.Yu. Ponomarev, J. Reif, A. Richter, C. Schlegel, R. Schwengner, S. Skoda, H.G. Thomas, I. Wiedenhover, G. Winter, A. Zilges, Phys. Lett. B **390**, 49 (1997).
4. K. Govaert, F. Bauwens, J. Bryssinck, D. De Frenne, E. Jacobs, W. Mondelaers, L. Govor, V.Yu. Ponomarev, Phys. Rev. C **57**, 2229 (1998).
5. R. Schwengner, R. Beyer, F. Dönau, E. Grosse, A. Hartmann, A.R. Junghans, S. Mallion, G. Rusev, K.D. Schilling, W. Schulze, A. Wagner, Nucl. Instrum. Methods A **555**, 211 (2005).
6. H.R. Weller, M.W. Ahmed, H. Gao, W. Tornow, Ying K. Wu, M. Gai, R. Miskimen, Prog. Part. Nucl. Phys. **62**, 257 (2009).
7. D. Savran, M. Babilon, A.M. van den Berg, M.N. Harakeh, J. Hasper, A. Matic, H.J. Wörtche, A. Zilges, Phys. Rev. Lett. **97**, 172502 (2006).
8. A. Tamii, I. Poltoratska, P. von Neumann-Cosel, Y. Fujita, T. Adachi, C.A. Bertulani, J. Carter, M. Dozono, H. Fujita, K. Fujita, K. Hatanaka, A.M. Heilmann, D. Ishikawa, M. Itoh, H.J. Ong, T. Kawabata, Y. Kalmykov, E. Litvinova, H. Matsubara, K. Nakanishi, R. Neveling, H. Okamura, B. Özel-Tashenov, V.Yu. Ponomarev, A. Richter, B. Rubio, H. Sakaguchi, Y. Sakemi, Y. Sasamoto, Y. Shimbara, Y. Shimizu, F.D. Smit, T. Suzuki, Y. Tameshige, J. Wambach, R. Yamada, M. Yosoi, J. Zenihiro, Phys. Rev. Lett. **107**, 062502 (2011).
9. F.C.L. Crespi, A. Bracco, R. Nicolini *et al.*, Phys. Rev. Lett. **113**, 012501 (2014).
10. D. Savran, V. Derya, S. Bagchi, J. Endres, M.N. Harakeh, J. Isaak, N. Kalantar-Nayestanaki, E.G. Lanza, B. Löher, A. Najafi, S. Pascu, S.G. Pickstone, N. Pietralla, V.Yu. Ponomarev, C. Rigollet, C. Romig, M. Spieker, A. Vitturi, A. Zilges, Phys. Lett. B **786**, 16 (2018).
11. N. Ryezayeva, T. Hartmann, Y. Kalmykov, H. Lenske, P. von Neumann-Cosel, V.Yu. Ponomarev, A. Richter, A. Shevchenko, S. Volz, J. Wambach, Phys. Rev. Lett. **89**, 272502 (2002).
12. G.F. Bertsch, P.F. Bortignon, R.A. Broglia, Rev. Mod. Phys. **55**, 287 (1983).
13. A. Bracco, E.G. Lanza, A. Tamii, Prog. Part. Nucl. Phys. **106**, 360 (2019).
14. N. Pietralla, Nucl. Phys. News **28**, 4 (2018) (for a recent laboratory portrait).
15. M.C.A. Campos, P. von Neumann-Cosel, F. Neumeyer, A. Richter, G. Schrieder, E. Spamer, B.A. Brown, R.J. Peterson, Phys. Lett. B **349**, 433 (1995).
16. H. Miska, H.D. Gräf, A. Richter, D. Schüll, E. Spamer, O. Titze, Phys. Lett. B **59**, 441 (1975).
17. H.D. Gräf, V. Heil, A. Richter, E. Spamer, W. Stock, O. Titze, Phys. Lett. B **72**, 179 (1977).
18. G. Kühner, D. Meuer, S. Müller, A. Richter, E. Spamer, O. Titze, Phys. Lett. B **104**, 189 (1981).
19. H. Diesener, U. Helm, G. Herbert, V. Huck, P. von Neumann-Cosel, C. Rangacharyulu, A. Richter, G. Schrieder, A. Stascheck, A. Stiller, J. Ryckebusch, J. Carter, Phys. Rev. Lett. **72**, 1994 (1994).
20. H. Diesener, U. Helm, P. von Neumann-Cosel, A. Richter, G. Schrieder, A. Stascheck, A. Stiller, J. Carter, Nucl. Phys. A **696**, 272 (2001).
21. H. Diesener, U. Helm, V. Huck, P. von Neumann-Cosel, C. Rangacharyulu, A. Richter, G. Schrieder, A. Stascheck, S. Strauch, J. Ryckebusch, J. Carter, Nucl. Phys. A **696**, 293 (2001).
22. J. Carter, H. Diesener, U. Helm, G. Herbert, P. von Neumann-Cosel, A. Richter, G. Schrieder, S. Strauch, Nucl. Phys. A **696**, 317 (2001).

23. S. Strauch, P. von Neumann-Cosel, C. Rangacharyulu, A. Richter, G. Schrieder, K. Schweda, J. Wambach, Phys. Rev. Lett. **85**, 2913 (2000).
24. P. Papakonstantinou, V.Yu. Ponomarev, R. Roth, J. Wambach, Eur. Phys. J. A **47**, 14 (2011).
25. P. Papakonstantinou, H. Hergert, V.Yu. Ponomarev, R. Roth, Phys. Lett. B **709**, 270 (2012).
26. P.-G. Reinhard, W. Nazarewicz, Phys. Rev. C **87**, 014324 (2013).
27. C. Lüttge, C. Hofmann, J. Horn, F. Neumeyer, A. Richter, G. Schrieder, E. Spamer, A. Stiller, D.I. Sober, S.K. Matthews, L.W. Fagg, Nucl. Instrum. Methods A **366**, 325 (1995).
28. H. Überall, *Electron Scattering from Complex Nuclei* (Academic Press, New York, 1971).
29. J. Heisenberg, H.P. Blok, Annu. Rev. Nucl. Part. Sci. **33**, 569 (1983).
30. A.J.F. Siegert, Phys. Rev. **52**, 787 (1937).
31. K. Govaert *et al.*, Nucl. Instrum. Methods A **337**, 265 (1994).
32. D. Savran, M. Elvers, J. Endres, M. Fritzsche, B. Löher, N. Pietralla, V.Yu. Ponomarev, C. Romig, L. Schnorrenberger, K. Sonnabend, A. Zilges, Phys. Rev. C **84**, 024326 (2011).
33. V.G. Soloviev, *Theory of Atomic Nuclei: Quasiparticles and Phonons* (Institute of Physics, Bristol, 1992).
34. N. Lo Iudice, V.Yu. Ponomarev, Ch. Stoyanov, A.V. Sushkov, V.V. Voronov, J. Phys. G: Nucl. Part. Phys. **39**, 043101 (2012).
35. V.Yu. Ponomarev, J. Phys.: Conf. Ser. **533**, 012028 (2013).
36. S.T. Tuan, L.E. Wright, D.S. Onley, Nucl. Instrum. Methods **60**, 70 (1968).
37. C.M. Vincent, H.T. Fortune, Phys. Rev. C **2**, 782 (1970).
38. D.H. Jakubassa-Amundsen, V.Yu. Ponomarev, Eur. Phys. J. A **52**, 48 (2016).
39. D.R. Yennie, D.G. Ravenhall, R.N. Wilson, Phys. Rev. **95**, 500 (1954).
40. D. Meuer, G. Kühner, S. Müller, A. Richter, E. Spamer, O. Titze, W. Knüpfer, Phys. Lett. B **106**, 289 (1981).